# Cu ion substitution induced grain growth, band gap engineering and carrier recombination engineering of all-inorganic $CsPbBr_3$ perovskite films

FEI ZHAO[1,*], WEILONG XU[1], YINGJIE ZHANG[1], YIXIN GUO[2,*], PEIZHI YANG[3], JUNHAO CHU[4]
[1]*School of Photoelectric Engineering, Changzhou Institute of Technology, Changzhou, Jiangsu, 213002, China*
[2]*Department of Physics, Shanghai Normal University, Shanghai 200233, China*
[3]*Key Laboratory of Advanced Technique & Preparation for Renewable Energy Materials, Ministry of Education, Yunnan Normal University, Kunming 650500, China*
[4]*Shanghai Institute of Technical Physics, Chinese Academy of Sciences, Shanghai 200083, China*

All-inorganic $CsPbBr_3$ perovskite films with the different degrees of Cu ion substitution were prepared by multi-step spin coating precursor solutions. Based on the results of XRD and XPS, it was confirmed that partial Pb was replaced by Cu and no impurities were generated with the increase of Cu content in the Cu-doped $CsPbBr_3$ film. The red shift of the diffraction peak and the decrease of lattice constant in the range of 0%-3% Cu ions in this XRD spectra demonstrate the progressive substitution of Cu ions, which suggests lattice contraction. It was seen that the average grain size significantly increased to 841.94 nm with the addition of 3% Cu into $CsPbBr_3$ films from SEM. Meanwhile, the optical band gap of the $CsPbBr_3$ film decreases to 2.336 eV and the recombination probability of carriers of the $CsPbBr_3$ film is lower when the Cu ion content gradually increases to 3%. However, the average grain size reduces, the optical band gap increases, and the recombination probability of carriers improves as the Cu ion content gradually increases to 6%. Therefore, the content of optimal Cu ion is 3% in this experiment. This work provides a new path for the development of all-inorganic perovskite films and devices.

(Received September 23, 2023; accepted February 9, 2024)

*Keywords*: All-inorganic $CsPbBr_3$ films, Cu-doping, Microstructure, Optical properties

## 1. Introduction

The organic-inorganic hybrid perovskite solar cell has attracted great interest due to its comprehensive advantages of high photoelectric conversion efficiency and low manufacturing cost. The efficiency of the organic-inorganic hybrid perovskite solar cell has been increased from 3.8% to 25.7% through ameliorating the quality of interface and perovskite films [1-5]. Despite the rapid development of the aforementioned hybrid device efficiency, they still have poor moisture and thermal stability. The reason behind this is that the hybrid perovskite absorption layer for the device has inferior stability towards air and heat [6], which inhibits their commercial application. Using inorganic materials to replace unstable organic components can effectively improve the stability of halide perovskite devices. Recently, the Cs-based all-inorganic perovskites ($CsSnI_3$, $CsPbI_3$, $CsPbI_2Br$, $CsPbIBr_2$, $CsPbBr_3$) have attracted great attention to enhance the stability of devices [7-11]. Among these all-inorganic perovskite materials, the $CsPbBr_3$ perovskite possesses the best stability [12]. Therefore, $CsPbBr_3$ perovskite films have been widely studied in solar cells.

An effective method to improve the quality of $CsPbBr_3$ perovskite films is to use a suitable preparation process. At present, the main methods for preparing $CsPbBr_3$ perovskite films include thermal evaporation method and multi-step spin coating method [13,14]. Previously, Some $CsPbBr_3$ films were prepared by thermal evaporation technology. Using this technology can prepare dense and uniform perovskite films. However, the manufacturing cost of the perovskite film obtained by the evaporation method is too high, which is not conducive to commercialization. In order to reduce the cost, the multi-step solution spin coating method is used to prepare $CsPbBr_3$ perovskite films [15]. The films prepared by this method have good density, uniformity and repeatability. Meanwhile, the manufacturing cost of the films prepared by the multi-step spin coating method is also extremely low. Thus, compared with evaporation method, the multi-step spin coating method is more suitable for preparing high-quality $CsPbBr_3$ perovskite films. Another effective method to enhance the quality of $CsPbBr_3$ perovskite films is to use ion doping. According to

previous reports, doping small ions into the perovskite lattice can effectively improve the crystallinity of the perovskite film, reduce the number of grain boundaries, and lessen defects [16]. Duan et al. first prepared $CsPbBr_3$ perovskite films with Sm ions [17]. Compared with undoped $CsPbBr_3$ perovskite films, Sm-doped $CsPbBr_3$ perovskite films can obtain larger grain size, smaller lattice constant and fewer grain boundaries. Afterwards, Zhao et al. introduced Sr ions into the $CsPbBr_3$ lattice and found that doping Sr ions can improve the crystallinity of $CsPbBr_3$ films, and reduce the lattice spacing and optical band gap of the films [18]. Their studies show that the ion-doped $CsPbBr_3$ films have excellent structural and optoelectronic properties. In order to further improve the quality of $CsPbBr_3$ film, it is necessary to seek other types of ion doping. To our knowledge, there is relatively little research on the influence of Cu ions on the structure and optical properties of $CsPbBr_3$ perovskite films.

In this work, Cu-doped $CsPbBr_3$ perovskite films are prepared by multi-step spin coating method. The results show that after incorporating an appropriate amount of Cu ions, the $CsPbBr_3$ films have larger average grain size, smaller lattice constants, fewer grain boundaries, smaller optical band gaps, and lower carrier recombination probability. By optimizing the Cu-doping concentration, we synthesize high-quality $CsPbBr_3$ films, which provides a basis for the research of efficient $CsPbBr_3$ solar cells.

## 2. Experimental

### 2.1. Deposition of thin films

FTO glasses were sequentially cleaned via ethanol and deionized water. For preparing undoped $CsPbBr_3$ perovskite films, the $CsPbBr_3$ films were deposited on the FTO glasses by multi-step spin coating method. 367 mg $PbBr_2$ (99.999%) in 1 mL N,N-dimethylformamide (DMF, 99.8%) solution was deposited on the FTO glasses at 2000 rpm for 30 s at 90 ℃, which results in the synthesis of $PbBr_2$ films. Then, the $PbBr_2$ films were annealed at 90 ℃ for 30 min. The 15 mg/mL CsBr (99.999%) methanol (99.9%) solution was immediately deposited on $PbBr_2$ films at 2000 rpm for 30 s. This process was repeated for four times. After deposition, each layer of CsBr methanol solution were annealed at 250 ℃ for 5 min. The $CsPbBr_3$ perovskite films was successfully prepared. For preparing Cu-doped $CsPbBr_3$ perovskite film, a certain amount of $CuBr_2$ (99.95%) is added to the DMF solution of $PbBr_2$. The other steps are consistent with the corresponding synthesis steps of the undoped $CsPbBr_3$ film.

### 2.2. Characterizations

The structures of perovskite films were characterized by the X-ray diffraction (XRD, D8 ADVANCE) diffractometer. The morphologies of perovskite films and energy-dispersive X-ray spectroscopy (EDS) mapping images were assessed via a field-emission scanning electron microscope (SEM, Quanta FEG 250). The perovskite grain size was measured from SEM images and a nano-measurement software. X-ray photoelectron spectroscopy (XPS, AXIS-Ultra DLD) spectra were gained to analyse the valence states of elements. Ultraviolet-visible (UV-vis) absorption spectra of perovskite films were obtained to analyse the optical bandgap of perovskite films. The photoluminescence (PL) spectra of perovskite films were tested under 325 nm wavelength excitation.

## 3. Results and discussions

### 3.1. Analysis of structure

The XRD patterns of the $CsPbBr_3$ perovskite films based on different Cu-doping concentrations are shown in Fig. 1a. All the $CsPbBr_3$ films exhibit the four diffraction peaks at 15.27°, 21.72°, 30.76° and 34.54°, which corresponds to the (100), (110), (200) and (210) planes of the $CsPbBr_3$ phase [19], respectively. In addition, there two obvious peaks at 24.46° and 37.86°, which is attribute to FTO [9]. In all planes of $CsPbBr_3$ phase, the intensity of (110) plane is the highest, which indicates that preferential orientation growth occurs during the growth process of $CsPbBr_3$ films. Fig. 1b shows partial enlarged XRD images of $CsPbBr_3$ perovskite films based on different Cu-doping concentrations. Fig. 1c shows intensity values of (110) diffraction peak. From Fig. 1b and Fig. 1c, it can be seen that as the Cu ion concentration improves from 0% to 3%, the (110) diffraction peak of $CsPbBr_3$ film gradually increases. This indicates increased crystallinity of $CsPbBr_3$ film. However, when the concentration of Cu-doping continues to increase from 3% to 6%, the (110) peak of $CsPbBr_3$ film decreases, which shows a reduction in the crystallinity of the $CsPbBr_3$ film. To further investigate the size variation of $CsPbBr_3$ films through XRD technology, the FWHM value of (110) peak needs to be discussed (Fig. 1d). The FWHM values of (110) peaks for the four samples of 0%, 1%, 3%, and 6% are 0.166, 0.158, 0.156, and 0.162, respectively. Among all the samples, the FWHM value of the 3% Cu-doped sample is the smallest, indicating that the average grain size of the 3% Cu-doped sample is the largest. Moreover, when the Cu- doping concentration increases from 0% to 3%, the (110) peak of $CsPbBr_3$ film shifts towards a large angle direction, indicating that Cu ions may incorporate into the lattice of $CsPbBr_3$ film. However, the (110) peak shifted towards a small angle direction as the Cu-doping concentration further increased to 6%, which is attributed to the influence of excessive Cu ions. To further verify whether Cu ions are successfully doped into the $CsPbBr_3$ lattice, we investigate the lattice constants of $CsPbBr_3$

films (Fig. 1e). The lattice constants for the Cu-doped $CsPbBr_3$ films of 0%, 1%, 3%, 6% are 5.781, 5.772, 5.772, and 5.784 Å, respectively. As shown in Fig. 1e, the lattice constant of $CsPbBr_3$ film decreases with the concentration improvement of Cu ions from 0% to 3%. The mechanism behind this phenomenon is that using smaller Cu ions (73 pm) to partially replace Pb ions (119 pm) can lead to lattice shrinkage [16]. This also indicates Cu ions have been successfully introduced into $CsPbBr_3$ lattice, which is consistent with the previous analysis results. In addition, excessive Cu ions (6%) can lead to reverse changes in lattice constants. In fact, lattice contraction is also favorable to stabilize the perovskite phase and increase the formation energy [20], which inhibits the formation of crystal nucleus and thus expands the grain size. Based on the previous analysis results, doping Cu ions in the $CsPbBr_3$ lattice is beneficial for improving grain size and reducing the number of grain boundaries.

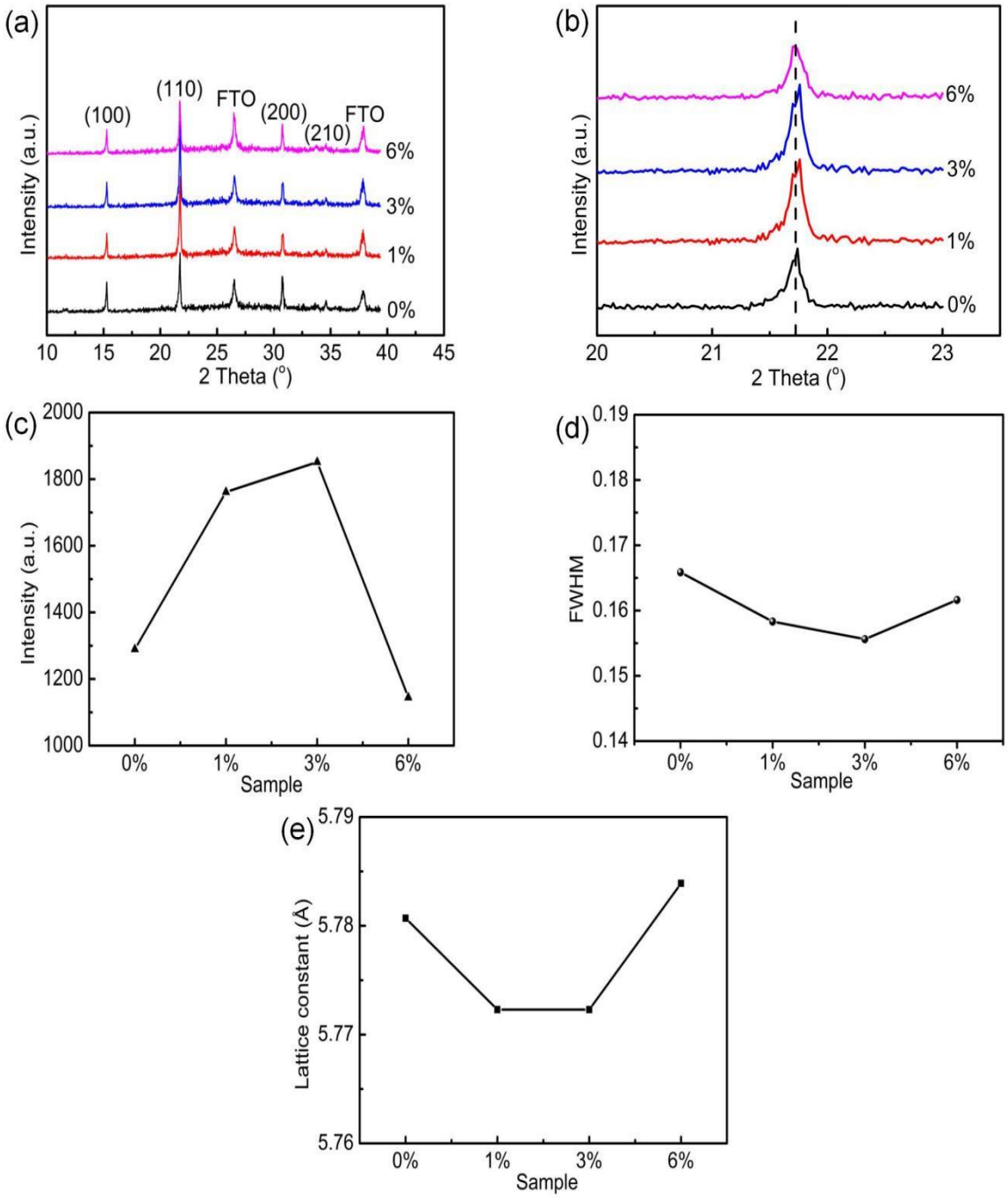


*Fig. 1. (a) XRD patterns of the $CsPbBr_3$ perovskite films with different Cu-doping concentrations. (b) Partial enlarged XRD images of $CsPbBr_3$ perovskite films based on different Cu-doping concentrations. (c) Intensity and (d) FWHM values of (110) diffraction peak. (e) Lattice constants of $CsPbBr_3$ perovskite films based on different Cu-doping concentrations (color online)*

### 3.2. Elemental valence state and morphology characterization

Fig. 2a shows XPS spectra (Pb 4f) of the $CsPbBr_3$ perovskite films with different Cu-doping concentrations. The peak position of Pb4f slightly shifts to higher bonding energy through doping Cu ions in $CsPbBr_3$ films, suggesting a change in the chemical states. The reason for the chemical state change of element is the redistribution of electron density caused by various binding interactions between $Cu^{2+}$ and $Br^-$ [18]. Fig. 2b indicates XPS spectra (Cu 2p) of the undoped and 3% Cu-doped $CsPbBr_3$ films. For undoped $CsPbBr_3$ film, there is no obvious diffraction peaks in the binding energy range of 930-933 eV. However, an obvious peak appears in the same binding energy range for 3% Cu-doped $CsPbBr_3$ film, indicating that Cu ions are incorporated into the lattice of $CsPbBr_3$ film and partial $Pb^{2+}$ sites are successfully replaced by $Cu^{2+}$.

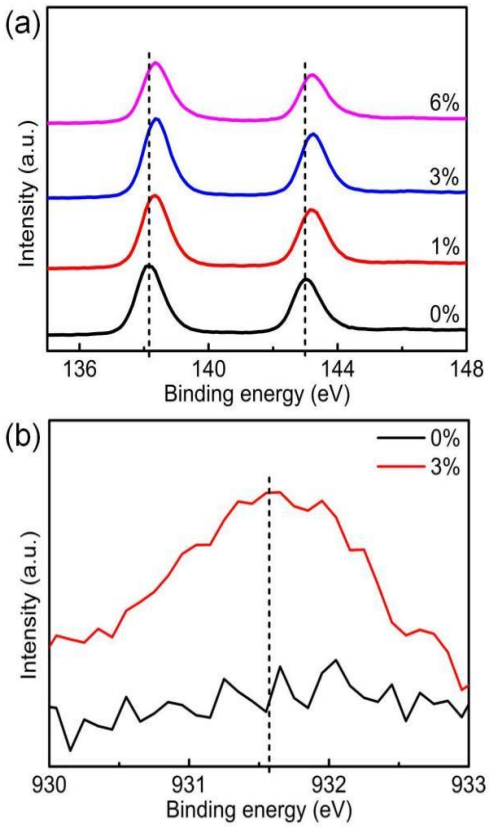


*Fig. 2. (a) XPS spectra (Pb 4f) of the $CsPbBr_3$ perovskite films with different Cu-doping concentrations. (b) XPS spectra (Cu 2p) of the undoped and 3% Cu-doped $CsPbBr_3$ perovskite films (color online)*

Fig. 3a-d shows SEM images of the Cu-doped $CsPbBr_3$ perovskite films with different Cu contents. The average grain size of $CsPbBr_3$ film increases from 551.82 nm to 841.94 nm when the Cu doping concentration increases from 0% to 3%. The reason for the increase in average grain size is due to lattice shrinkage caused by Cu ion doping. The continuous growth of $CsPbBr_3$ grains can decrease the number of grain boundaries and reduce defects [21]. However, as the Cu doping concentration further increases, the average grain size decreases to 467.99 nm. Meanwhile, a small number of pores appeare on the surface of $CsPbBr_3$ film. The above phenomenon indicates that the concentration of excessive Cu ion can inhibit grain growth [16]. To study the distribution of elements, EDS elemental mapping of the undoped and 3% Cu-doped $CsPbBr_3$ films was characterized (Fig. 4a and b). As shown in Fig. 4a and b, the 3% Cu-doped $CsPbBr_3$ film exhibits a uniform distribution of elements, indicating that the $CsPbBr_3$ film with the concentration of 3% Cu ion has good quality.

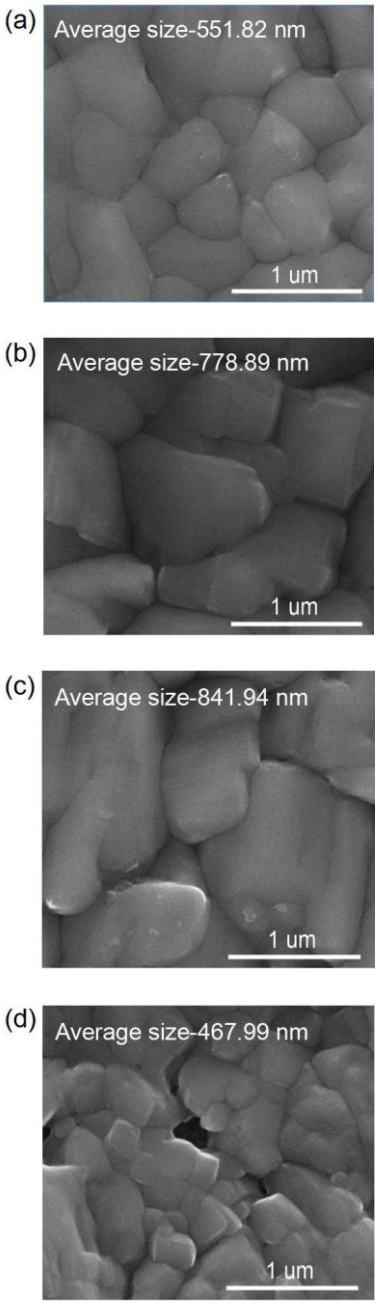


*Fig. 3. (a) SEM images of the Cu-doped $CsPbBr_3$ perovskite films with Cu contents of (a) 0%, (b) 1%, (c) 3% and (d) 6%*

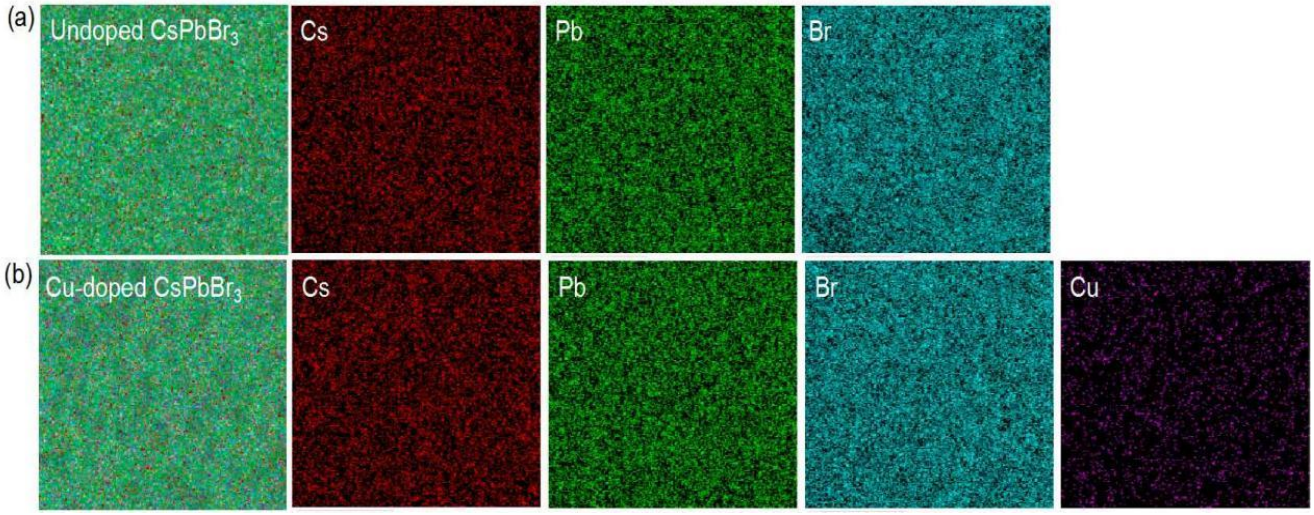


*Fig. 4. EDX elemental mapping of the (a) undoped and (b) 3% Cu-doped $CsPbBr_3$ perovskite films (color online)*

### 3.3. Analysis of optical performance

Fig. 5a shows ultraviolet visible light absorption spectrum of the $CsPbBr_3$ films with different Cu-doping concentrations. The absorption intensity of $CsPbBr_3$ film gradually increases as the concentration of Cu ions improves from 0% to 3%. However, when the Cu concentration of $CsPbBr_3$ film further increases to 6%, its absorption intensity begins to decrease. The above analysis indicates that when the concentration of Cu ions is 3%, the absorption intensity of the film is the highest. The improvement of absorption intensity for $CsPbBr_3$ film is attributed to its crystallinity enhancement. Fig. 5b shows plot of $(ahv)^2$ versus hv for the estimation of the band gap energy of the $CsPbBr_3$ films. According to the relationship between $(ahv)^2$ and hv, the optical band gap of $CsPbBr_3$ film can be obtained [22-25]. For undoped $CsPbBr_3$ film, it has the optical bandgap of 2.353 eV. For 3% Cu-doped $CsPbBr_3$ film, its optical bandgap is reduced to 2.336 eV. The decrease in the bandgap of the $CsPbBr_3$ film is attributed to the incorporation of Cu ions into the film. However, 6% Cu-doped $CsPbBr_3$ film has a higher optical bandgap (2.345 eV), which is due to the influence of excessive Cu ions. From the above results, it can be seen that when the content of Cu ion is 3%, the optical band gap for the $CsPbBr_3$ film is the smallest.

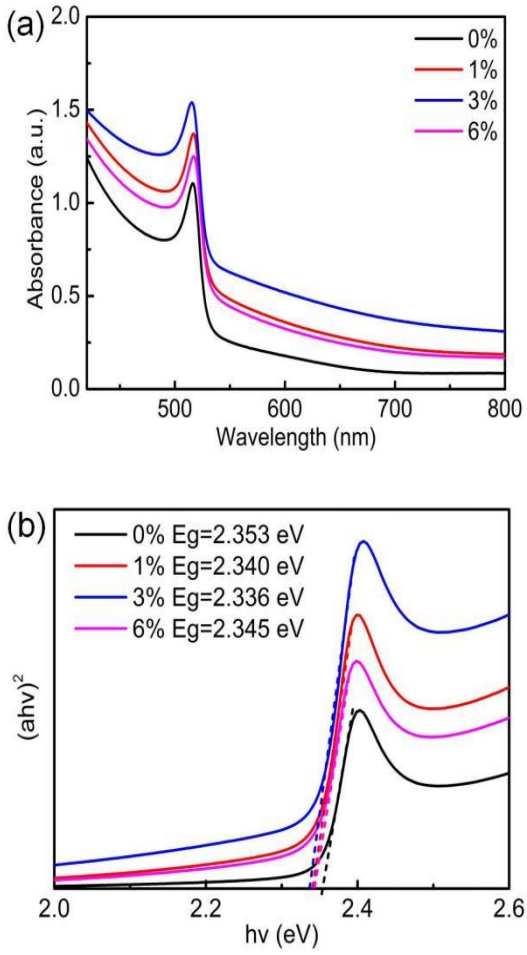


*Fig. 5. (a) Ultraviolet visible light absorption spectrum of the $CsPbBr_3$ perovskite films with different Cu-doping concentrations. (b) Plot of $(ahv)^2$ versus hv for the estimation of the band gap energy of the $CsPbBr_3$ perovskite films (color online)*

In order to further investigate the optical properties of the $CsPbBr_3$ film, the PL spectra with different Cu-doping concentrations were characterized, as shown in Fig. 6a. When the Cu ion content is within the range of 0%-3%, the intensity of PL luminescence peak for the doped $CsPbBr_3$ film with 3% Cu ion is the highest. The improvement of peak intensity indicates that the separation ability of carriers is enhanced and the recombination probability of carriers is decreased [26-30]. However, the PL peak intensity for 6% Cu-doped $CsPbBr_3$ film presents a decreasing trend, which shows an opposite pattern of change. After Cu ion doping, in addition to the change in PL peak intensity, there is also a small displacement for the PL peak position of $CsPbBr_3$ film. Fig. 6b shows peak position of the $CsPbBr_3$ films with different Cu-doping concentrations. As the content of Cu ions gradually increases to 3%, the PL peak of the $CsPbBr_3$ film undergoes a red shift. However, the PL peak appears a blue shift when the Cu ion content increases to 6%. The mechanisms behind the red shift and blue shift of the $CsPbBr_3$ films are the introduction of Cu ions and the action of excess Cu ions, respectively.

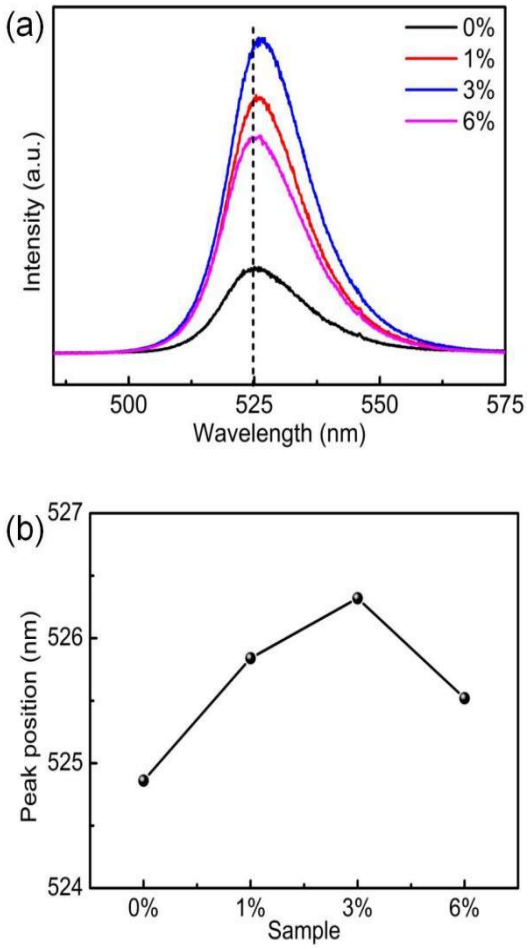


*Fig. 6. (a) PL spectra and peak position (b) of the $CsPbBr_3$ perovskite films with different Cu-doping concentrations (color online)*

## 4. Conclusions

Summarizing results presented above, all-inorganic $CsPbBr_3$ films with different contents of Cu were synthesized by multi-step spin coating method. The prepared films manifest outstanding structural and optical characteristics for promising all-inorganic perovskite solar cells. Cu ion substitution induces a red shift of the XRD main peak of $CsPbBr_3$ film with the improvement of Cu content, leading to a decrease in the calculated lattice constant. However, excessive Cu content can result in a blue shift of the XRD main peak and an increase in lattice constant. Meanwhile, the $CsPbBr_3$ film has a larger average grain size (841.94 nm), smaller optical band gap (2.336 eV), and lower recombination probability of carriers after an appropriate amount of Cu ions are incorporated into the $CsPbBr_3$ film. These findings offer a better understanding of Cu-doped $CsPbBr_3$, which is a promising way to prepare high-efficiency all-inorganic perovskite solar cells.

**Acknowledgements**

This work was financed by the National Natural Science Foundation of China (Grant No. 12304043), the National Natural Science Foundation of China (Grant No. U1802257), Spring City Plan: the High-level Talent Promotion and Training Project of Kunming (Grant No. 2022SCP005) and the Young Talent Program of Changzhou Institute of Technology (Grant No. 31020222006).

## References

[1] P. Luo, Y. Zhou, S. Zhou, Y. Lu, C. Xu, W. Xia, L. Sun, Chem. Eng. J. **343**, 146 (2018).
[2] K. Chen, P. Wu, W. Yang, R. Su, D. Luo, X. Yang, Y. Tu, R. Zhu, Q. Gong, Nano Energy **49**, 411 (2018).
[3] X. Yao, B. He, J. Zhu, J. Ti, L. Cui, R. Tui, M. Wei, H. Chen, J. Duan, Y. Duan, Q. Tang, Nano Energy **96**, 107138 (2022).
[4] J. Zhu, Y. Liu, B. He, W. Zhang, L. Cui, S. Wang, H. Chen, Y. Duan, Q. Tang, Chem. Eng. J. **428**, 131950 (2022).
[5] Y. Liu, T. Xiang, B. Zhang, J. Wang, X. Yu, Y. Xiao, J. Xiao, Z. Ku, Y. Peng, ACS Appl. Energy Mater. **5**, 8049 (2022).
[6] P. Teng, X. Han, J. Li, Y. Xu, L. Kang, Y. Wang, Y. Yang, T. Yu, ACS Appl. Mater. Interfaces **10**, 9541 (2018).
[7] G. Liao, J. Duan, Y. Zhao, Q. Tang, Sol. Energy **171**, 279 (2018).
[8] Y. Guo, F. Zhao, J. Tao, J. Jiang, J. Zhang, J. Yang, Z. Hu, J. Chu, ChemSusChem **12**, 983 (2019).

[9] X. Liu, X. Tan, Z. Liu, H. Ye, B. Sun, T. Shi, Z. Tang, G. Liao, Nano Energy **56**, 184 (2019).
[10] C. Wang, J. Zhang, L. Jiang, L. Gong, H. Xie, Y. Gao, H. He, Z. Fang, J. Fan, Z. Chao, J. Alloys Compd. **817**, 152768 (2020).
[11] J. Duan, Y. Zhao, B. He, Q. Tang, Small **14**, 1704443 (2018).
[12] Y. Liu, B. He, J. Duan, Y. Zhao, Y. Ding, M. Tang, H. Chen, Q. Tang, J. Mater. Chem. A **7**, 12635 (2019).
[13] H. Li, G. Tong, T. Chen, H. Zhu, G. Li, Y. Chang, L. Wang, Y. Jiang, J. Mater. Chem. A **6**, 14255 (2018).
[14] Y. Li, J. Duan, H. Yuan, Y. Zhao, B. He, Q. Tang, Solar RRL **2**, 1800164 (2018).
[15] H. Guo, Y. Pei, J. Zhang, C. Cai, K. Zhou, Y. Zhu, J. Mater. Chem. C **7**, 11234 (2019).
[16] M. Tang, B. He, D. Dou, Y. Liu, J. Duan, Y. Zhao, H. Chen, Q. Tang, Chem. Eng. J. **375**, 121930 (2019).
[17] J. Duan, Y. Zhao, X. Yang, Y. Wang, B. He, Q. Tang, Adv. Energy Mater. 1802346 (2018).
[18] Y. Zhao, Y. Wang, J. Duan, X. Yang, Q. Tang, J. Mater. Chem. A **7**, 6877 (2019).
[19] F. Zhao, Y. Guo, J. Tao, Z. Li, J. Jiang, J. Chu, Appl. Optics **59**, 5481 (2020).
[20] M. T. Klug, A. Osherov, A. A. Haghighirad, S. D. Stranks, P. R. Brown, S. Bai, X. Dang, V. Bulović, H. J. Snaith, A. M. Belcher, Energy Environ. Sci. **10**, 236 (2017).
[21] G. Tong, T. Chen, H. Li, L. Qiu, Z. Liu, Y. Dang, W. Song, L. K. Ono, Y. Jiang, Y. Qi, Nano Energy **65**, 104015 (2019).
[22] X. Tan, X. Liu, Z. Liu, B. Sun, J. Li, S. Xi, T. Shi, Z. Tang, G. Liao, Appl. Surf. Sci. **499**, 143990 (2020).
[23] Z. Xu, X. Yin, Y. Guo, Y. Pu, M. He, J. Mater. Chem. C **6**, 4746 (2018).
[24] P. Karuppuswamy, C. Hanmandlu, K. M. Boopathi, P. Perumal, C. Liu, Y. Chen, Y. Chang, P. Wang, C. Lai, C. Chu, Sol. Energy Mater. Sol. Cells **169**, 78 (2017).
[25] Z. Zhou, Y. Deng, P. Zhang, D. Kou, W. Zhou, Y. Meng, S. Yuan, S. Wu, Solar RRL **3**, 1800354 (2019).
[26] W. Zhang, J. Xiong, J. Li, W. A. Daoud, Small **16**, 2001535 (2020).
[27] D. Wang, W. Li, Z. Du, G. Li, W. Sun, J. Wu, Z. Lan, J. Mater. Chem. C **8**, 1649 (2020).
[28] D. Wang, W. Li, Z. Du, G. Li, W. Sun, J. Wu, Z. Lan, ACS Appl. Mater. Interfaces **12**, 10579 (2020).
[29] X. Cao, G. Zhang, Y. Cai, L. Jiang, X. He, Q. Zeng, J. Wei, Y. Jia, G. Xing, W. Huang, Solar RRL **4**, 2000008 (2020).
[30] A. Singh, S. Najman, A. Mohapatra, Y. Lu, C. Hanmandlu, C. Pao, Y. Chen, C. S. Lai, C. Chu, ACS Appl. Mater. Interfaces **12**, 32649 (2020).

*Corresponding author: fzhaobs@126.com;
yxguo@shnu.edu.cn